HYDROLOGICAL PROCESSES
Hydrol. Process. **27**, 2004–2020 (2013)
Published online 23 May 2012 in Wiley Online Library
(wileyonlinelibrary.com) DOI: 10.1002/hyp.9354

Delineation of saltwater intrusion zones using the time domain electromagnetic method: the Nabeul–Hammamet coastal aquifer case study (NE Tunisia)

Fatma Trabelsi,[1]* Abdallah Ben Mammou,[1] Jamila Tarhouni,[2] Carlo Piga[3] and Gaetano Ranieri[3]

[1] *Faculty of Sciences of Tunis, Mineral Resources and Environment Laboratory, Department of Geology, University Tunis El Manar, 2092 Tunis El Manar, Tunisia*

[2] *National Institute of Agronomy of Tunisia (INAT), Sciences and Technology of Water Laboratory, Department of Rural Engineering, University 7 November, 43 Avenue Charles Nicolle, 1082 Tunis, Tunisia*

[3] *Faculty of Engineering of Cagliari, Geophysics Laboratory, Department of Territorial Engineering, University of Cagliari, P.zza d'Armi 16, 09123, Cagliari, Italy*

Abstract:

The time domain electromagnetic method (TDEM) is applied to monitor, to delineate and to map the saltwater intrusion zones in the Mediterranean Plio-Quaternary aquifer. Forty-two TDEM soundings were carried out in the coastal plain of Nabeul–Hammamet region (NE Tunisia). TDEM resistivity data were correlated with the existing borehole logging data to assign them to a particular lithology and to provide information about the position of the freshwater–seawater transition zone. The geoelectric sections showing the vertical configuration of seawater intrusion, with the brackish-salty-saturated zones, have a resistivity ranging from ~0.1 to 5 Ω·m and are detected at a depth lower than 1.5 m. The salinized zones are located at Nabeul (Sidi Moussa, Sidi El Mahrsi, Al Gasba and Mrazgua) and at Hammamet (Touristic zone of Hammamet north and south, Baraket Essahel) and reached a distance of 4 km from the coastline, indicating a severe state for the aquifer in these zones. These TDEM results are confirmed by the increase of chloride concentration content in the analysed water samples of monitoring wells. Moreover, in the northeastern part, the presence of a saltwater front located far from the coast and along the NW–SE major surface fault can be explained by two hypothesis: (i) this fault seems to provide a conduit for seawater to move readily towards the water wells and (ii) the clay and gypsum infiltration of marine Messinian deposits through the fault plane leads to low resistivities. Finally, it comes out from this study that TDEM survey has successfully depicted salinized zones of this coastal aquifer. Copyright © 2012 John Wiley & Sons, Ltd.

KEY WORDS TDEM; saltwater intrusion; Plio-Quaternary aquifer; Nabeul–Hammamet; Tunisia

Received 10 March 2011; Accepted 20 April 2012

INTRODUCTION

Groundwater is a vital resource for socioeconomic development in coastal areas worldwide. The water demands of these areas have increased during the last decades because of rapid urbanization, accelerated tourism development, agricultural activities and a continuous population growth (Xue *et al*., 1993). Water needs are mainly covered by groundwater abstracted from the aquifers via numerous wells and boreholes. As a result, a negative water balance is established in coastal aquifer systems, triggering seawater intrusion. It occurs when the sea, with interesting permeable rocks (for porosity or fractures), creates an interface below freshwaters according to density contrast and aquifer geometry. Therefore, pinpointing the interface position as precisely as possible is extremely important. The most direct method for determining the location of the saline wedge is to measure water conductivity at different depths until an abrupt variation in salinity is detected (Duque *et al*., 2008). However, in detrital coastal aquifers, freshwater is usually encountered at shallow depths, and most water monitoring wells and boreholes are often too shallow to intersect the interface. Test boreholes are drilled to monitor the advance of the saline wedge, which is prohibitively costly because special drilling techniques must be used due to the lack of cohesion in the detrital sediments of these aquifers. Contrariwise, geophysical techniques offer a suitable method for determining the location of the freshwater–seawater interface because costs are reduced and results are good. Moreover, these methods also provide complementary information on the characteristics of the interface and the sediments forming the aquifer.

The evaluation of seawater intrusion has been dealt with through a variety of geophysical techniques for which it would be useful to know the subsurface resistivity to estimate the saline water intrusion, and geoelectric and geoelectromagnetic techniques are the leading ones (Goldman and Neubauer, 1994, Kafri and Goldman, 2005). These techniques are particularly efficient in the exploration of saline groundwater due

*Correspondence to: Fatma Trabelsi, Faculty of Sciences of Tunis, Mineral Resources and Environment Laboratory, Department of Geology, University Tunis El Manar, 2092 Tunis El Manar, Tunisia.
E-mail: trabelsifatma@gmail.com

to the close relation between salinity and electrical resistivity/conductivity measurements. It helps in understanding spatial relations between fresh, brackish and saline water, which commonly coexist in coastal aquifers. The large differences between the resistivity of saltwater-saturated zones and the freshwater-saturated zones have been used by several investigations to determine the saltwater intrusion in many coastal areas (Hodlur *et al*., 2010; Van Dam and Meulenkamp 1967; De Breuk and De Moor 1969; Zohdy 1969; Sabet, 1975; Ginsberg and Levanton 1976; Urish and Frohlich 1990; and Frohlich *et al*., 1994).

In most cases, the application of the geophysical methods has focused on studying the geometrical features of the target (e.g. the depth to freshwater–saline groundwater interface). This problem was successfully treated by all relevant methods. Direct current (DC) electrical imaging is one of the most efficient and powerful technique to map freshwater–saltwater interfaces. Many geoelectrical surveys based on the one-dimensional (1D) vertical electrical sounding (VES) were performed in different coastal areas around the world (e.g. Urish and Frohlich 1990; Ebraheem *et al*., 1997; Nowroozi *et al*., 1999; Choudhury and Saha 2004). Also, many studies based on the two-dimensional (2D) ERT technique are also reported (Nassir *et al*., 2000; Wilson *et al*., 2005; Sherif *et al*., 2006). Moreover, the time domain electromagnetic method (TDEM) has been used successfully in hydrogeological surveys, geological mapping applications, aquifer structure delineation and contamination (Raiche, 1984, Hoekstra and Bloom, 1986, Goldman *et al*., 1991). The method has been extensively applied in studies of seawater intrusion and soil and groundwater salinization. Paine (2003) used time domain and frequency domain electromagnetic techniques to outline zones affected by soil salinization and to estimate the total subsurface chloride mass. In a series of articles, Goldman *et al*. (1991), Kafri *et al*. (1997), Yechieli *et al*. (2001) and Kafri and Goldman (2005) present the application of the TDEM method to map and delineate seawater intrusion phenomena in the Mediterranean and Dead Sea coastal aquifers. Nevertheless, the TDEM was particularly accurate and efficient in detecting seawater intrusion because of its highest sensitivity to electrically conductive targets, best vertical and lateral resolutions and highest depth-to-array size characteristics compared with the rest of geophysical techniques (Fitterman and Stewart, 1986; Kafri and Goldman, 2005).

However, this case study demonstrates the use of TDEM survey correlated with borehole geophysical logging data to detect and monitor saltwater intrusion in the typical Mediterranean coastal aquifer. Indeed, the northeastern coast of Tunisia is both threatened by seawater intrusion and seepage of pollutants that are degrading the groundwater quality (Paniconi *et al*., 2001; Kouzana *et al*., 2009; Kerrou *et al*., 2010). However, the case study chosen is the Nabeul–Hammamet (NH) area, located in the northeastern of Tunisia, in the eastern part of the Cap Bon peninsula (Figure 1). It encompasses an area of approximately 330 km^2, 27 km in length and from approximately 6 to 18 km in width, bordered by the Korba region in the east, the Bouficha area in the west, the Grombalia zone in the north and the Mediterranean Sea along the south (Figure 1). The study area is characterized by a semiarid climate with an average annual precipitation of 456 (1997–2009) and an annual mean evaporation intensity of 1189 mm (1985–2004). The region is heavily populated and is considered an interesting area both for its tourist attractions as well as its significant urban, agricultural and industrial activities.

The steady increase in water consumption has severely depleted the shallow aquifer, reduced water levels, led to saltwater encroachment and dewatered some areas of this coastal plain. To face this threat, several measures were taken by the Tunisian state, such as prohibiting the construction of new wells (the region has been declared a protected area since 1941), developing alternative sources of freshwater, building dams and water bypasses from the north of the country, distributing efficient irrigation systems and reusing treated waste water for artificial recharge of the aquifer (e.g. Oued Souhil pilot station).

Furthermore, this report focuses to more precisely define the position of the freshwater–seawater transition zones, to locate the extent of salinized zones and to map the shallow aquifer of NH coastal aquifer system.

Geological setting

The coastal plain of NH is located in the western coast of the Sicilian Strait (Elmejdoub and Jedoui, 2009). It has a very complex geological structure and variable outcropping with lateral and vertical facies variation due to polydirectional syn-sedimentary faults. The oldest outcrops are allotted to the lower Eocene, whereas the most recent are allotted to old and recent Quaternary (Ben Salem, 1992) (Figures 1 and 2). This coastal area is bounded by a group of steep relieves; Mounts Batin, Al Hshish and Hammamet in the northeast; Mounts El Guedim, El Mhissa and El Menchar in the northwest; and Quaternary marine platforms in the south. The first elevated mountains make a monocline structure (Ben Salem, 1992) occupied by detrital deposits of upper Miocene (Colleuil, 1976) and transgressive marine sediments of Pliocene. The latter were unconformably deposited on the folded and eroded formations of Miocene, and the lower Miocene, Oligocene and upper Eocene deposits outcrop along the western part of the basin (Burollet, 1956; Blondel, 1991). Throughout the middle part is shown a NW–SE-directed structure that corresponds to Grombalia graben covered by Quaternary sediments (Castany, 1948) and giving the area a synclinal shape bordered by major faults towards the northwest (Ben Ayed, 1986; Chihi, 1995; Turki, 1985). The southern part of the area is mainly constituted by quaternary deposits, which are usually composed of two units: the lower unit of marine facies, corresponding to the sandy limestone of the Tyrrhenian transgression, and the upper unit, mainly

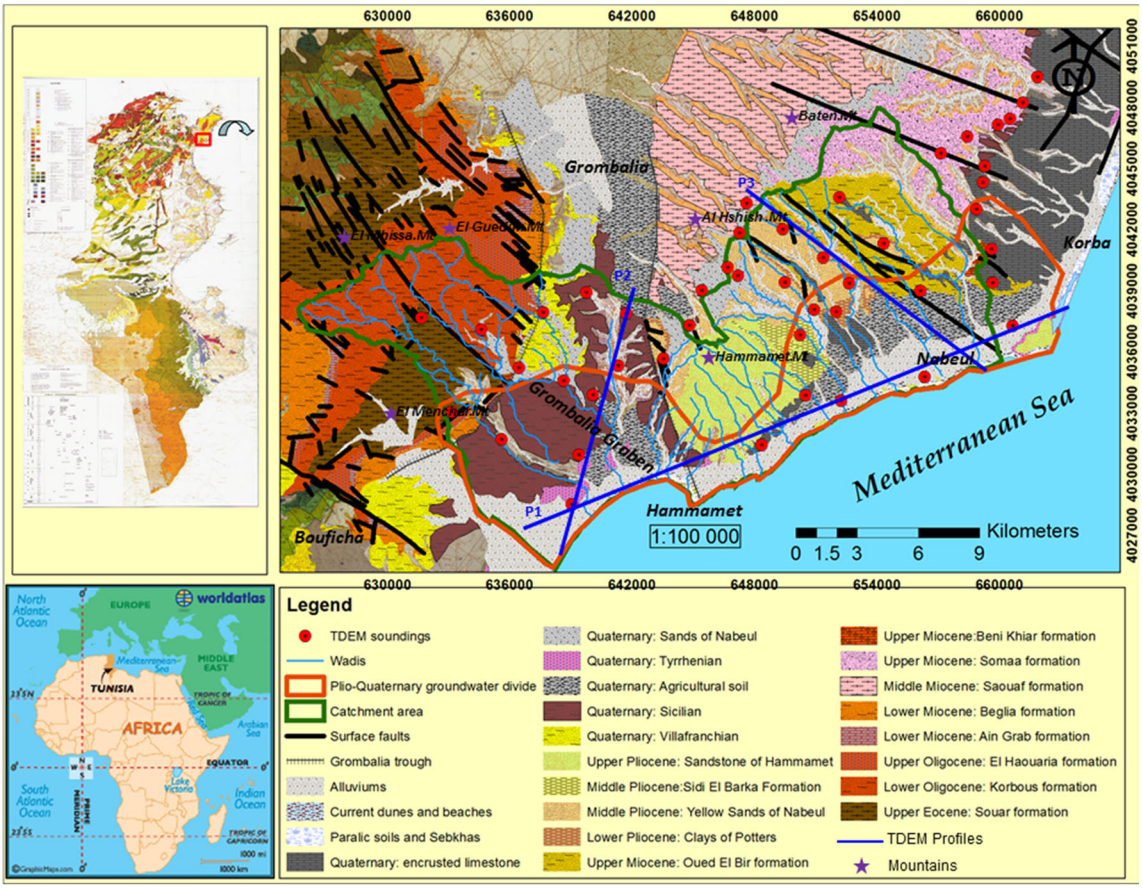

Figure 1. NH location map, showing regional geology and location of TDEM soundings and profiles

composing continental facies (Ozer *et al.*, 1980). These deposits form nowadays coastal consolidated dunes built by wind marine regression (Chakroun *et al.*, 2005; Ozer *et al.*, 1980). The old consolidated dunes cover the Tyrrhenian deposits (Ozer *et al.*, 1980). The encrusted limestone extends over significant distances (Ben Salem,

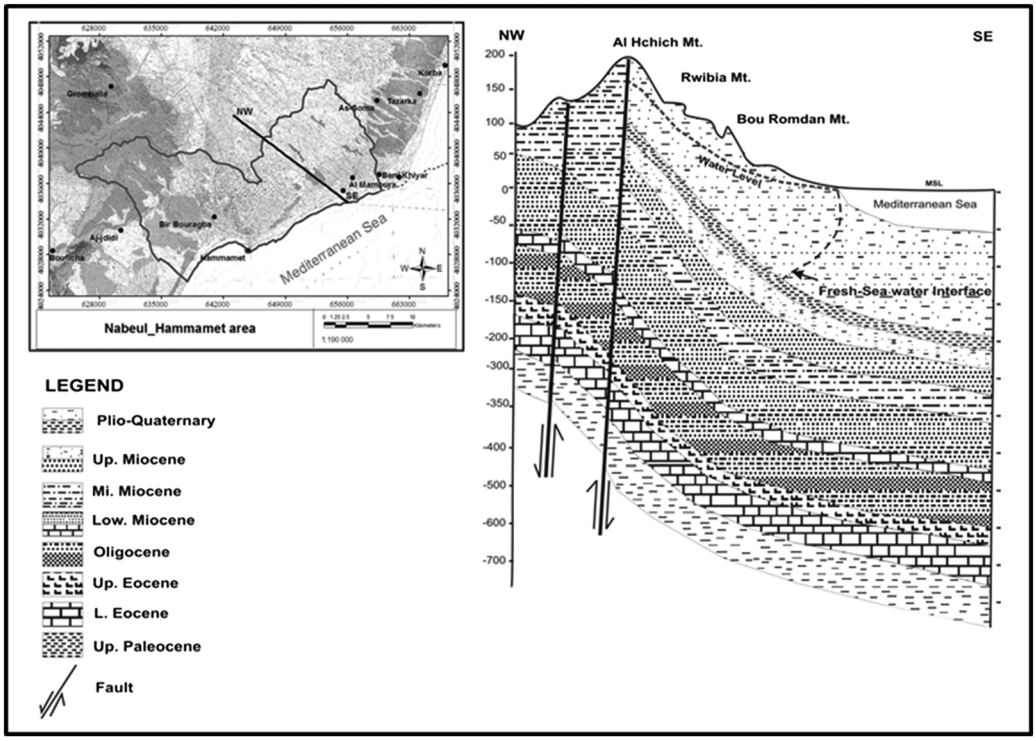

Figure 2. Geological cross section (NW–SE)

1992). Finally, The Holocene deposits form the recent alluvia of rivers (wadis), current dunes and beaches. These alluvial deposits, often terraced, are characterized by different permeability degrees by the grain size and a generally medium–high pollution vulnerability.

Hydrogeological setting

From a hydrological point of view, the surface drainage network in NH catchment area is very dense (Figure 4) and is constituted by several nonperennial wadis, in which the most important are Oued Souhil and Oued El Kebir in the east and Oued el Batin and Oued Sidi Hammed in the west. This hydrological network supplies a multilayer aquifer system in which the recharge by surface water bodies is quantified approximately 11.18 Mm^3/year (DWR, 2005). In addition, this aquifer system is being recharged through the excess of surface irrigation water and water leaks from the Medjerda open channel, the artificial recharge of the groundwater level by reuse of treated waste water (at Oued Souhil pilot station) and the interaquifer flow. Then, it is discharged through outflow into the drainage system, direct abstraction, evapotranspiration, interaquifer flow of groundwater processes, groundwater returning flow to the wadis and drains and extraction by wells. In the NH aquifer system, it is possible to distinguish four principal geostructural complexes, characterized by hydrogeological heterogeneity: the Plio-Quaternary aquifer, the Miocene aquifer, the Oligocene aquifer and the Eocene aquifer (Trabelsi *et al*., 2011). Nevertheless, the most important regional shallow aquifer in NH is the Plio-Quaternary reservoir, which is the purpose of this study (Figures 2 and 3). The quaternary units Alluviums, Old soil, Sicilian, Tyrrhenian and Villafranchian form together a discontinuous semiunconfined multilayer aquifer interconnected by sandy clay aquitards. In the upper part of the catchment area, the Quaternary aquifer is unconfined and is hydraulically connected to the hydrological network, whereas the aquifer turns into a multilayered system downstream as the intercalations of clay are getting thicker. Hydraulic gradient, hydraulic conductivity and transmissivity present a large range of variation because of changes in grain size and local increases of clay content, which vary in thickness and are laterally discontinuous. Therefore, the Pliocene aquifer flows between the sandy sandstone deposits of 'Sandstone of Hammamet' formation and 'Yellow Sands of Nabeul' formation. The first unit aquifer is found in the Hammamet region and is thicker in the north than that in the south, approximately 20 to 200 m. In the southwestern riverside of Oued Souhil to the north of Hammamet, the second Pliocene aquifer is unconfined, with 60 to 140 m of thickness, and turns into multilayer towards the southern part. The bedrock of the Plio-Quaternary reservoir is constituted by the Pliocene clayey deposits (the Potters clay and/or Sidi El Barka formations), which separate this groundwater reservoir from the underling confined aquifers of the Miocene, Oligocene and Eocene deposits.

The piezometric map (2006) (Figure 4) of the shallow water table shows that groundwater flows converge from northwest to southeast and from the northeast towards the Mediterranean Sea, which constitute the natural discharge area. This highlights the recharge of the unconfined aquifer in the foot of the mountains. In addition, this map shows a multidirectional flow mainly oriented to the piezometric depressions, locally reaching levels of −5 m. These depressions are located in the western part at the south of Hammamet and in the eastern part at the El Maamoura region.

METHODOLOGY

The principal methodology adopted in this article is the use of TDEM survey to detect salinized zones and to monitor seawater intrusion. Nevertheless, with reference to different workers who have attempted the study of seawater intrusion by geophysical methods (Ginsberg and Levanton, 1976; Goldman *et al*., 1991; Paine, 2003; Kafri and Goldman, 2005; Duque *et al*., 2008; Hodlur *et al*., 2010), the intrusion phenomena and the background resistivity picture make the interpretation of the resistivity data very difficult. The more challenging part of the interpretation is the attempt to link the low-resistivity zones to possible seawater intrusion. The pore fluid, which can be a mixture of freshwater and seawater with varying proportion, will be embedded in the pores of the host rock, which will have different resistivity corresponding to the mineral composition. In the study

AGE	STAGE	FORMATION		LITHOLOGY	AQUIFERS & SUBSTRATUMS
Quaternary	Holocene	Alluvium		Sandy-Silty deposits	Aquifer
		Agriculture Soil		Sandy deposits	Aquifer
		Screen of Sands		Sand pack	Aquifer
		Calcareous crust		Calcareous crust	
	Tyrrhenian			Sandy Limestone	
	Sicilian			Conglomerates sand and Clay	Aquifer
	Villafranchian			Clay, gravel, sand, clayey sand, sandstone, marl	Aquifer
Pliocene	Upper Pliocene: Plaisancian	Sand and Sandstone of Hammamet		Sand with sandstones bars	Aquifer
	Middle Pliocene: Tabianian	Clays of Sidi El Barka		Argillaceous deposits	Substratum
	Lower Pliocene: Zanclean	Yellow Sand of Nabeul		Sandy deposits	Aquifer
		Potters Clay		Clayey deposits	Substratum

Figure 3. Hydrogeological chart of the Plio-Quaternary reservoir

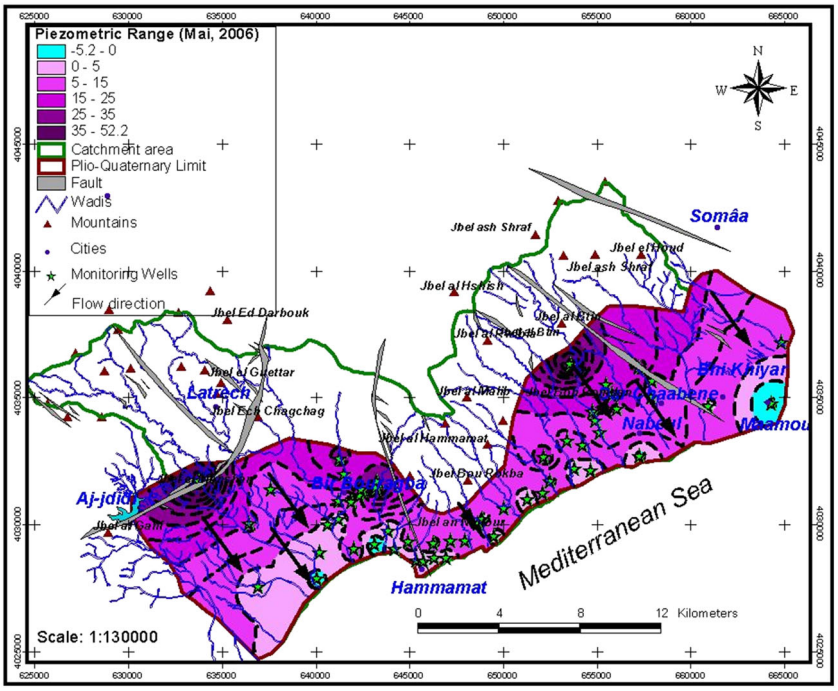

Figure 4. Piezometric map of the shallow aquifer (May, 2006)

area, the clayey sand forms the principal host rock, and the seawater and the freshwater are embedded in the pores. Then, the presence of dispersed or interbeded clay will suppress the bulk resistivity of the aquifer. The interpretation was performed on the basis that the very low resistivity images could be attributed to the seawater intrusion or clay. Hence, it will be misleading to attempt an interpretation totally based only on the TDEM results. The wireline logging data of boreholes are used to help, to assess the quality of the TDEM soundings and to identify lithological formations in the stratigraphic column. In addition, the concentration values of chloride from the water samples of boreholes, located near the TDEM soundings, have been used to verify the relationship between the lithological units and the measured resistivity.

TDEM survey

The TDEM method has been used in environmental and hydrogeologic studies, but its main requirement is the ability to accurately detect the freshwater–saline water interface and to determine the bulk resistivity of the aquifer below the interface (Kafri and Goldman, 2005). This method was routinely used to detect the intruding saline water bodies during the last 20 years.

A detailed description of the method is given by Danielsen *et al.* (2003) and belongs to the category of controlled source EM methods. The TDEM method makes use of a DC transmitted into the transmitter loop lying on the ground. The current creates a primary, stationary magnetic field. The DC is switched off, which induces an eddy current system in the ground. Because of the ohmic resistance of the subsurface, the current system will decay and further induce a secondary magnetic field that is measured in an induction coil (the receiver coil). The decay rate of the electromagnetic field depends on the resistivity distribution of the subsurface. The field decay is slower in a conductive medium than in a resistive medium. The importance of the TDEM method lies on the measurement time of the transient response. As already mentioned, the induced voltage at Rx (receiver) loop is measured after the Tx (transmitter) loop was turned off, which means that we measure a secondary response in the absence of the primary field. This approach produces results less sensitive to errors of Tx/Rx geometry. There is no need for complicated tools to separate the primary signal, and the Tx/Rx separation has a small effect in the exploration depth (contrary to conventional controlled source methods). These features produce results with the highest lateral resolution. Consequently, the TDEM method has an excellent depth resolution of conductive layers, whereas the resolution of resistive layers is limited (Christensen and Sørensen 1998). TDEM soundings are usually made with loop size ranging between 25 and 300 m, depending on the exploration target. The penetration depth is dependent on the magnetic moment of the equipment (i.e. transmitter loop size and number of turns and the transmitted current), the resistivity of the ground and the magnitude of electromagnetic background noise (Macnae *et al.*, 1984; McCracken *et al.*, 1986).

The advantages of TDEM are the good sensitivity to conductive formations, the depth of investigation that is greater than the transmitter loop side length, the best lateral and vertical resolution with regard to highly conductive targets (Kaufman and Keller, 1983) and the convenience of not requiring any galvanic contact with the ground. The main disadvantages are poor sensitivity to resistive formations and shallow near surface layers (Figure 5; Everett and Meju 2005; Ernstson and Kirsch 2006a).

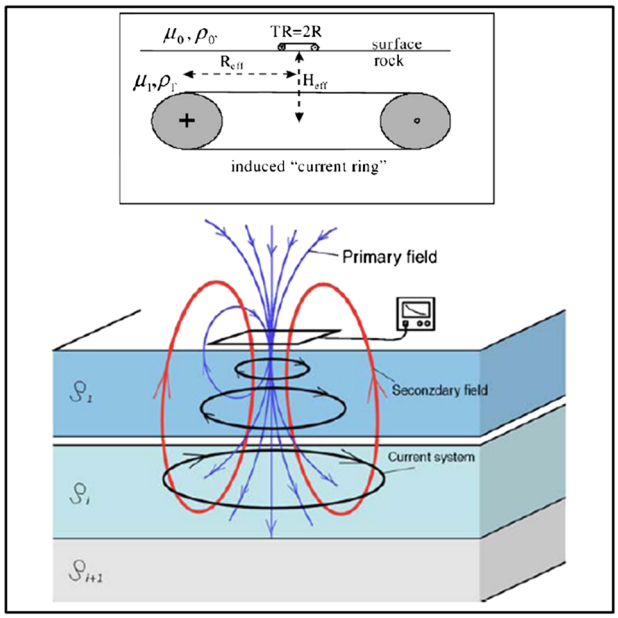

Figure 5. Physical principle of the TDEM. A stationary current flowing in the transmitting loop creates a primary magnetic field. After this current is shut off, a secondary current is induced in the subsurface, which creates secondary magnetic field, measured in the receiving coil

TDEM data acquisition and processing

The TDEM sounding technology enables to conduct subsurface soundings to a depth of 300 m, depending on the frequency used (lower frequencies sense deeper into the ground) and the geological formation (deeper for a freshwater-saturated zone than for a seawater intruded zone). In this work, the measurements were made with a TEM FAST 48 battery-powered transmitter (4–16 ms), connected to a single-turn, ungrounded and insulated cable in the form of a square loop with sides of between 25 and 300 m. This instrument was used because of the following characteristics: precision, ease of handling and rapidity of acquisition. However, 42 TDEM sounding locations (Figure 1) were occupied with the coincident loop configuration (50×50- and 100×100-m square loops at 50- and 100-m spacing, respectively) aligned on a rectangular grid. Two approaches were adopted for selecting sounding locations and surveying strategy: (i) potential sounding locations were first selected based on site size, and selected sites had to be large enough to accommodate the 50-m^2 transmitter loop geometries proposed; and (ii) the locations that were sufficiently large for conducting a TDEM survey were then evaluated on the basis of accessibility (road access and owner permission) and proximity to cultural features such as power lines and metallic water distribution pipelines that may distort the electromagnetic fields and bias the interpretation.

Indeed, the voltage/time transients were recorded and transformed to resistivity versus time. After the acquisition, the TDEM collected data were edited, smoothed, analysed and processed using the TEM-Researcher software (Fainberg, 1999). Although, numerous measurements and studies (e.g. Goldman, 1988; Paine, 2003) correlated TDEM resistivities with groundwater salinities. These studies have shown that in most cases, the portions of the aquifer saturated with seawater have resistivity values within a range of 1 to 3 Ω·m. The portions of the aquifer saturated with brackish waters (transition or mixing zone) exhibit resistivities between 3 and 10 Ω·m, and fresh groundwater bodies show higher resistivities. Observations from all around the world show similar resistivity values for saline water–saturated rocks, and most important, they also show that almost any lithologies, whether freshwater saturated or dry, exhibit much higher resistivities (Palacky, 1987). This fact enables the delineation of seawater intrusion along the length of a coastal aquifer (Goldman *et al.*, 1991) and is used, in this study, as a guideline for the interpretation of vertical resistivity logs, 2D geoelectric sections and depth slices (resistivity maps).

Borehole data

The borehole logging data are used to calibrate the processed data of TDEM soundings and to identify the lithological formations. Borehole logging is the process of measuring the physical, chemical and structural properties of penetrated geological formations usually using logging tools that are lowered into a borehole on a wireline cable. Geophysical downhole logging is an important and strong tool in hydrogeology, for example, for constructing regional or local geological models of groundwater reservoirs and for evaluation of borehole condition and water-producing fractures at a detailed scale. Borehole logging is the most certain and exact way to locate lithology changes; hence, geophysical logging is important in combination with, for example, seismic investigations and other surface geophysical measurements (vertical electrical sounding, TDEM, etc.) for geological modelling. Further, it is very important in combination with groundwater sampling from, for example, monitoring wells when delineating saltwater intrusion or pollution plumes. The application of geophysical well logging methods have been dealt with by several publications over the last several years: hydrogeological investigations (Repsold 1989, Mares *et al.*, 1994, Jorgensen & Petricola 1995, Kobr *et al.*, 2005), coastal aquifers and freshwater–saltwater boundaries (Buckley *et al.*, 2001, Hwang *et al.*, 2004).

In this study, various wireline logging data of 160 water boreholes are provided by the local groundwater management authority (CRDA Nabeul). These borehole data including radioactivity logging (natural gamma, gamma–gamma) and electrical logging (Self Potential (SP), Electric Log (EL) and Microlog (ML)) were used for analyzing hydrogeological characteristics, identifying the type of lithological formation, calibrating the TDEM processed data and finally interpreting the 2D geoelectrical section. The TDEM soundings were conducted wherever possible at a maximum distance of 1 km of existing water boreholes, allowing the correlation of TDEM resistivity log with borehole logging.

However, the passive radioactivity measurements (Meyers, 1992) allow to distinguish between sand and clay layers and to estimate the clay content. The electrical well logs, such as a self-potential tool (SP) and a resistivity log (electric log EL and microlog ML), are used in open holes to determine the electrical resistivity of the rock, which together with other physical parameters can be used to derive a lithological log for the borehole (Maute 1992, Spies 1996).

RESULTS: INTERPRETATION

One-dimensional interpretation

A variety of TDEM data interpretation techniques have been proposed. These include the imaging techniques (Keller and Frischknecht, 1966; Ranieri, 2000), conductive finite plate models (Keating and Crossley, 1990; Nabighian, 1979) and inversion methods that use 1D horizontal layered earth model (Christensen, 1995; Constable, 1987; Goldman, 1988; Raiche, 1984). Despite the popularity of TDEM method, which is typically applied from either ground-based or airborne platforms, TDEM data have mainly been interpreted using 1D layered earth models. There are two main reasons for this: (i) the subsurface can be conceptualized as a layered structure in many cases and (ii) the fully 3D forward simulation of the TDEM signal propagation is computationally challenging and CPU time intensive. In contrast, 1D layered earth TDEM forward modelling can be performed semianalytically using integral transforms and digital filtering (Gottwein *et al*., 2010).

The voltage/time transients were transformed to resistivity/time and inverted into 1D layered models (Fainberg, 1999). Smooth models were produced using a modified Occam inversion (Constable *et al*., 1987). No constraints (on depths or resistivities) were applied to any of the layered models. The depth of the regional water level and the freshwater lens thickness known from a preexisting water supply borehole are provided on the basis of the starting model.

Nevertheless, an example of a 1D interpretation of TDEM sounding is given in Figures 6a and 6b. Figure 6a shows that the field raw data were edited (e.g. first points were excluded from the curve for further analysis) and smoothed before the modelling. The TEM-Researcher software provides two ways of processing the TDEM sounding: transformation and inversion. Figure 6b shows the transformation resistivity (Res (h)), which is the distribution of specific resistivity versus apparent depth (smooth curve) and the model after 1D inversion (piecewise uniform diagram).

The interpretation of resistivity vertical log reveals that most of the sites that yield sounding curves show a monotonic decrease in apparent resistivity with time. Such curve behaviour undoubtedly proves the presence of a low-resistivity layer in the base of the section. At some sites, it was necessary to include a thin layer of very low resistivity within the top resistive layer to be consistent with the data. However, the quantitative interpretation of TDEM measurements is hampered by the equivalence problem, which means that several different layered models may give practically the same resistivity curve. To choose the model that best represents actual subsurface conditions, supplementary data such as borehole logging are used. Consequently, a correlation between TDEM resistivity logs and borehole logging was established. Moreover, TDEM method is most effective when the resistivity data can be calibrated with the analytic results of water samples from monitoring wells and boreholes. In this study, chloride concentration data are correlated with TDEM resistivity measurements.

Indeed, Figure 7 shows the correlation between the TDEM resistivity logs (T35 and T16) and the wireline logging (Gamma-Ray (GR), Self Potential (SP) and Electrical resistivity) of two boreholes (IRH 12500 and IRH 12545). These are located near Hammamet (Figure 7a) and Nabeul (Dar Chaabene) (Figure 7b) and at approximately 850 m and 2 km from the coast, respectively. Figure 7a shows that below the surface soil layer, gamma counts range between 10 and 50 cps, indicating predominantly sands and sandstones around the borehole (Keys 1997). Electrical resistivity values range from approximately 0 to 30 Ω·m, and the TDEM resistivity values range between 0.1 and 6 Ω·m. In the unsaturated zone (0–10 m), gamma counts range from slightly higher than 20 to 40 cps over a range of electrical resistivity values between 23 and 28 Ω·m and TDEM resistivity values approximately 1 to 6 Ω·m. The abrupt shift in both electrical and TDEM resistivity curves at the water table (−10.5 m) is immediately apparent. The apparent negative correlation between gamma cps and resistivity values was shown in the saturated zone (10–37 m), where gamma counts range from 10 to 40 cps over a range of electrical resistivity values approximately 15 to 20 Ω·m and TDEM resistivity values between 0.1 and 2 Ω·m. In addition, the relatively sharp decrease in resistivity in both electrical and TDEM resistivity logging at the depth (−40 m) mentions a relative transition zone. In addition, clayey sand and sandy silt sequences were identified on the basis of a noticeable increase in gamma count, which persist vertically at a depth greater than 50 to 100 m. The presence of dispersed or interbeded clay will suppress the bulk resistivity of the aquifer. The relatively high GR count in the borehole log reflects the clay-rich nature of the aquifer in this area. Low-resistivity measurements on both the TDEM sounding and the electrical log represent the combined effects of clay content and high salinity conditions within the NH aquifer at this station. Moreover, the analytic result of the water sample of this borehole shows a chloride concentration value of 1075 mg/l, which support the hypothesis of contamination by seawater intrusion.

Therefore, in the borehole IRH 12545, the presence of saline/or brackish water in sand (25–30 m) sediments around and in the borehole is obvious. The GR, electrical and TDEM resistivity log curves indicate lower values ranging between 20 and 30 cps, between 20 and 40 Ω·m and between 3 and 10 Ω·m, respectively. This persisted for the lower part (32–100 m) of the main aquifer at this

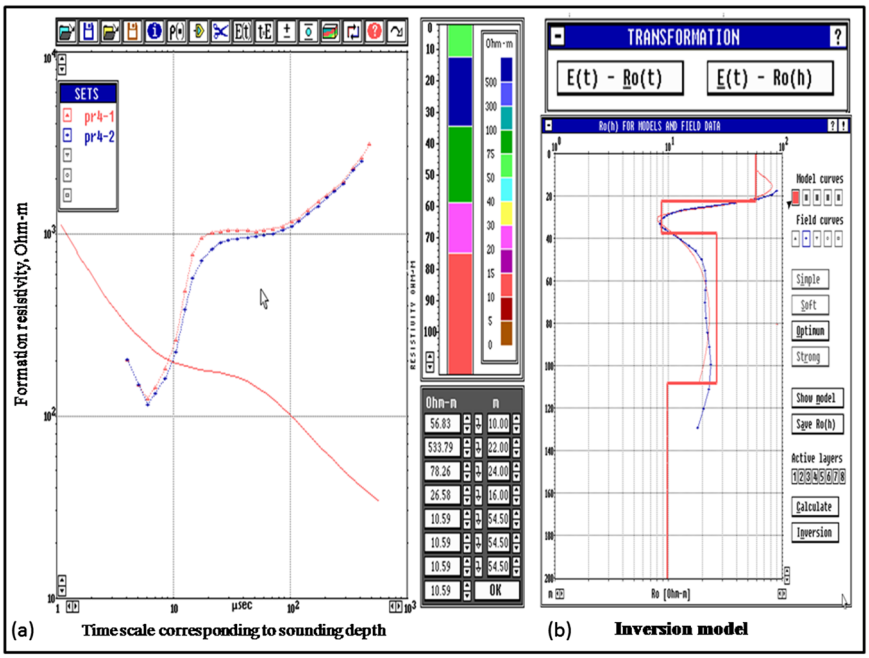

Figure 6. Example of a real field sounding curve with inversion results of the formation resistivity profile

site. Thus, the upper 30 m of the main aquifer (10–30 m below surface) contains freshwater. A sudden significant fall in both the electrical and the TDEM resistivity logs is observed at a depth of approximately 32 m. This may indicate a transition zone of freshwater–seawater interface. Also, the chloride content of analysed water sample is of approximately 877 mg/l.

Finally, the transition zone separating freshwater and seawater is recognizable between 30 and 35 m depth in Figure 7a and between 25 and 30 m depth in Figure 7b.

However, the correlation between wireline logging data of coastal neighbouring boreholes (IRH 13208, IRH 11644, IRH 11736, IRH 12500, IRH 13242 and IRH 12545), TDEM logs and lithologic columns was con-

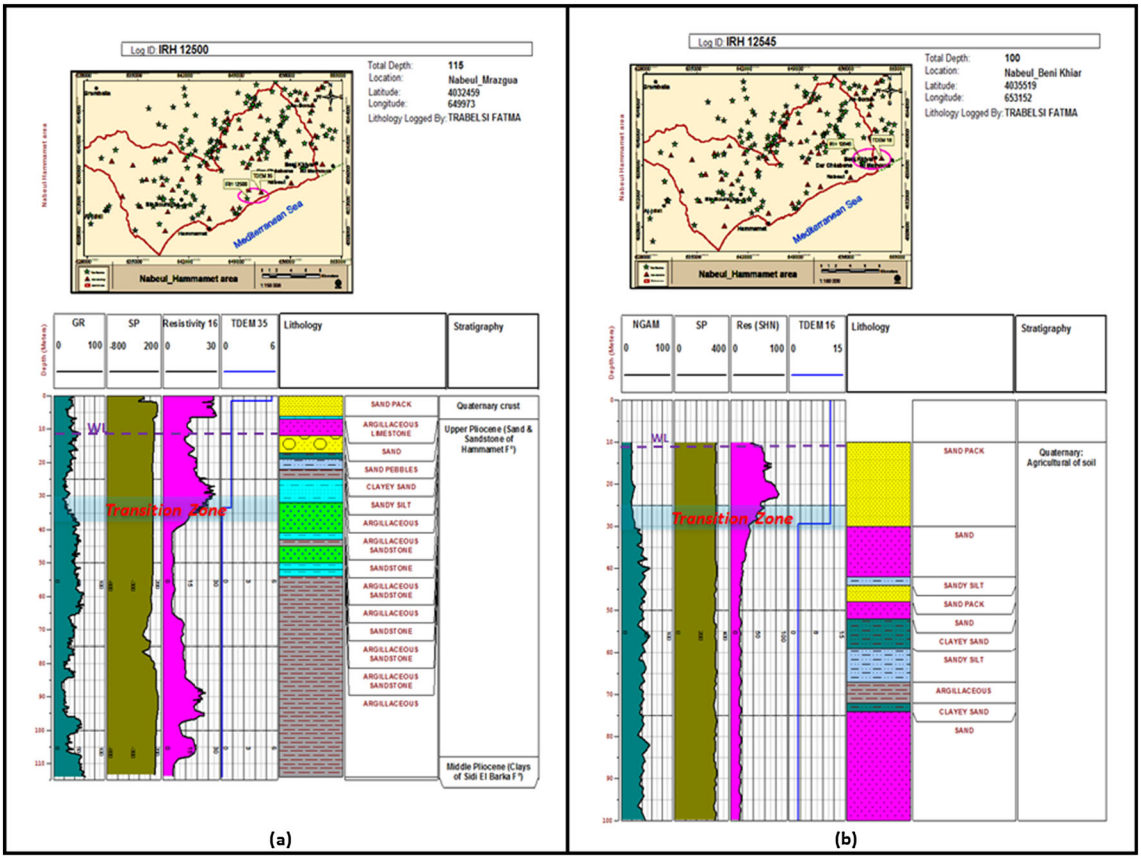

Figure 7. Correlation between TDEM resistivity logs and borehole logging data (GR, SP and resistivity)

ducted to show the freshwater–seawater transition zone. In the following parts, 2D geoelectrical sections were made to support this interpretation (Figure 8).

Two-dimensional geoelectrical sections

The geoelectric sections were established on the basis of the TDEM soundings interpreted with the assumption of a 1D structure and correlated with the borehole logging data. These cross sections were drawn using the results of interpretation with a minimum number of layers. All the measured stations are processed and plotted along profiles to show the resistivity distribution with depth and distance, to define the geometry of the aquifer, to identify the structures and to map the transition zone of freshwater–seawater and saltwater wedge.

Figure 9 shows a west–east, dip-parallel profile 1 (P1) (Figure 1), comprising seven TDEM soundings, starting from sounding T31 on the far west end to sounding T16 on the far east end of the profile, which extends to approximately 39 km. This coastal geoelectrical section highlights the presence of three water zones (Figure 9). Near the surface interval, a high-resistivity zone of 10 to 31 Ω·m and a thickness range between 36 and 72 m appear, indicative of freshwater zone (A). The lithology nature of this zone is clayey sand with encrusted limestone grounds, which constitute the accumulation zone of water and a preferred path of water draining. The second water zone has a resistivity and thickness that ranged between 3 and 10 Ω·m and between 34 and 57 m, respectively, characterized by sandy clay and sandy deposits and can be classed as brackish water zone (B). The third water zone (C) of clayey sand and sandy sediments has a low-resistivity layer with 1 to 3 Ω·m and could be attributed to saline water zone. It is noticeable that the freshwater–seawater interface is clearly indicated on this cross section. The rise almost to the surface of seawater intrusion is clearly showing in TDEM soundings T8, T31, T35 and T36. Finally, it shows at the deeper portion of the section, a very low resistivity zone (D) with 0.1 to 1 Ω·m due to high salinity conditions. By contrast, any hydro-lithostratigraphic detail is almost completely masked in this interval of depth, where low-resistivity, highly saline aquifers are difficult to distinguish from intervening clays. However, the salinity of groundwater is usually the predominant influence on TDEM resistivity measurements (Goldman *et al.*, 1991); thus, TDEM records do not always lend themselves well to lithostratigraphic correlation. In the shallower part of a TDEM profile, the distinctions can be often shown between the high resistivity of freshwater aquifers and the low resistivity of clays in the intervening confining beds.

To show the continuity of the seawater intrusion, a NE–SW geoelectrical section (Figure 10) was constructed from a transversal profile (P2) (Figure 1), crossing the quaternary deposits of Grombalia Graben. This comprises five TDEM soundings, starting from sounding T20 on the far northeast end to sounding T31 on the far southwest end of the profile, which extends to approximately 12 km. This cross section shows a relatively high-resistivity zone of 10 to 32 Ω·m with a thickness range between 55 and 90 m, which gets shallower southward and disappears near the coast. This zone is constituted by clayey sand interceded with bedded clay and considered as freshwater zone (zone A). There is also a relatively medium resistivity shallow layer with 3 to 10 Ω·m and thickness approximately 20 to 76 m, attributed to clayey sandstone and sandy sediments saturated with brackish water (zone B). Also in greater depth, a high-resistivity layer ranging from 12 to 32 Ω·m appears (zone E). However, because of the lack of hydro-lithostratigraphic data in this portion of section, this resistivity can be explained by the existence of deeper confined aquifer formations or resistive deposits. Although towards the coast, it shows the Quaternary alluvium deposits saturated with salty

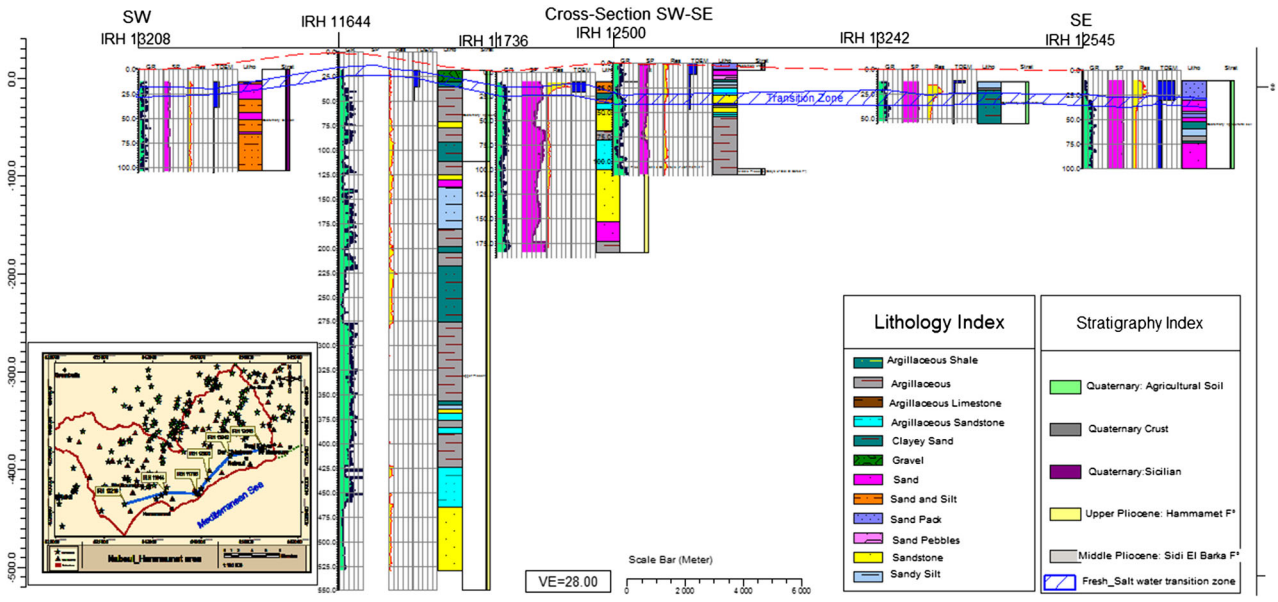

Figure 8. Cross section of correlation between borehole logging data, TDEM logs and lithological columns

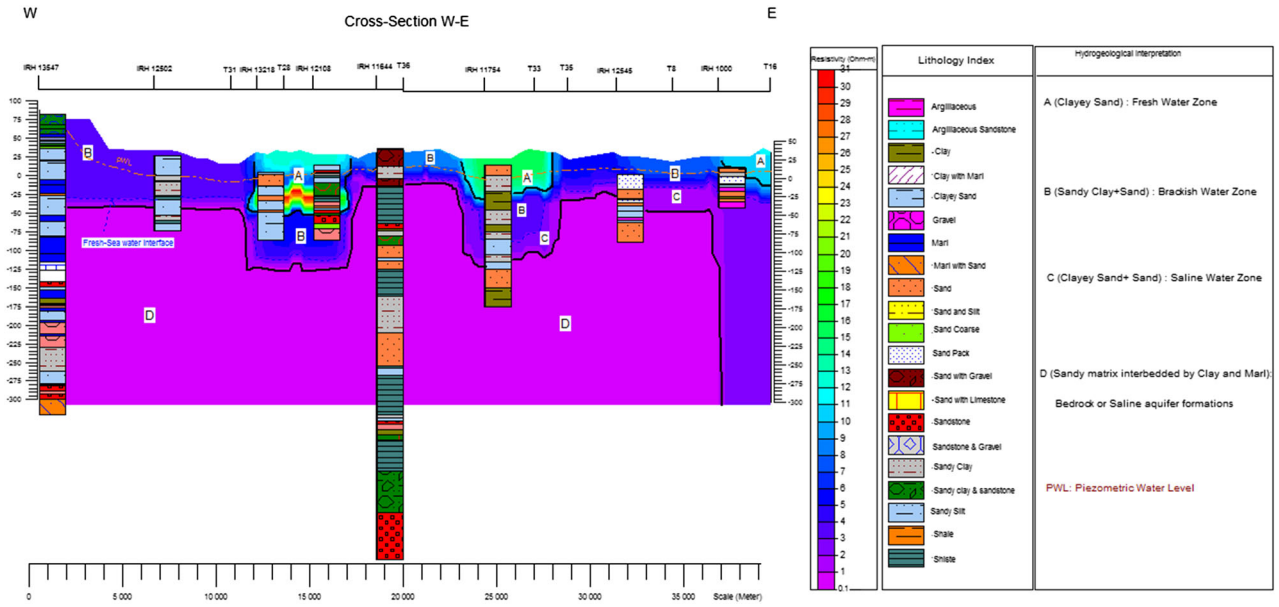

Figure 9. Geoelectrical section (P1)

water with a resistivity range of 0.1 to 3 Ω·m (zone D). Hence, this section illustrates the appearance of an important salinized zone in the coast of Hammamet Sud.

Figure 11 shows the geoelectrical section constructed from the profile (P3) (Figure 1) perpendicular to the coast and parallel to NW–SE major fault (Ben Salem and Colleuil, 1991). It comprises six TDEM soundings, starting from sounding T4 on the far northwest end to sounding T8 on the far southeast end, which extends to approximately 18 km. From the northwestern side, it shows a surface horizon made of sandy deposits (upper Pliocene) characterized by medium resistivities (10–27 Ω·m). This stratum is saturated with more or less freshwater (zone A). Towards the coast, this horizon passes laterally to sandy deposits of the Quaternary alluvium saturated with brackish to salty water (zone B), with a resistivity ranging between 3 and 10 Ω·m. Therefore, a low-resistivity zone (3–5 Ω·m) rich in clay and marl (zone C) may contain salts washed from the surface and concentrated at greater depth. This zone can constitute the substratum of the aquifer formation and then shows a very low resistivity zone towards the coast (0.1–3 Ω·m) (zone D), extending from few metres to a depth greater than 150 m. This zone can be attributed to seawater intrusion zone. Also, there is in a deeper section a very high resistivity layer of approximately 30 to 90 Ω·m with thickness upper than 100 m, rich in sand, sand with marl and sand with limestone which. In addition, because of the lack of hydrostratigraphic details, this zone may present freshwater aquifer formations or resistive deposits.

This low- to high-resistivity variation of freshwater zone can be explained by the lateral effect of the cited fault, although the resistivity within a fracture zone is in general lower than the resistivity of the host rock. The low-resistivity most probably reflects the changes associated with fault zones (e.g. shearing, shale smearing,

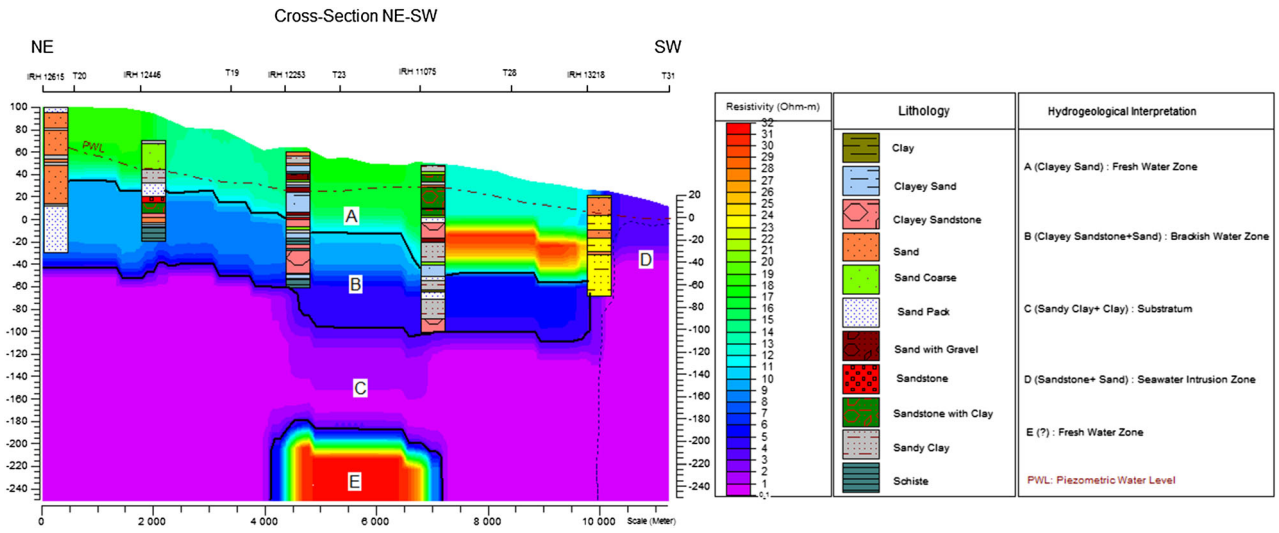

Figure 10. Geoelectrical section (P2)

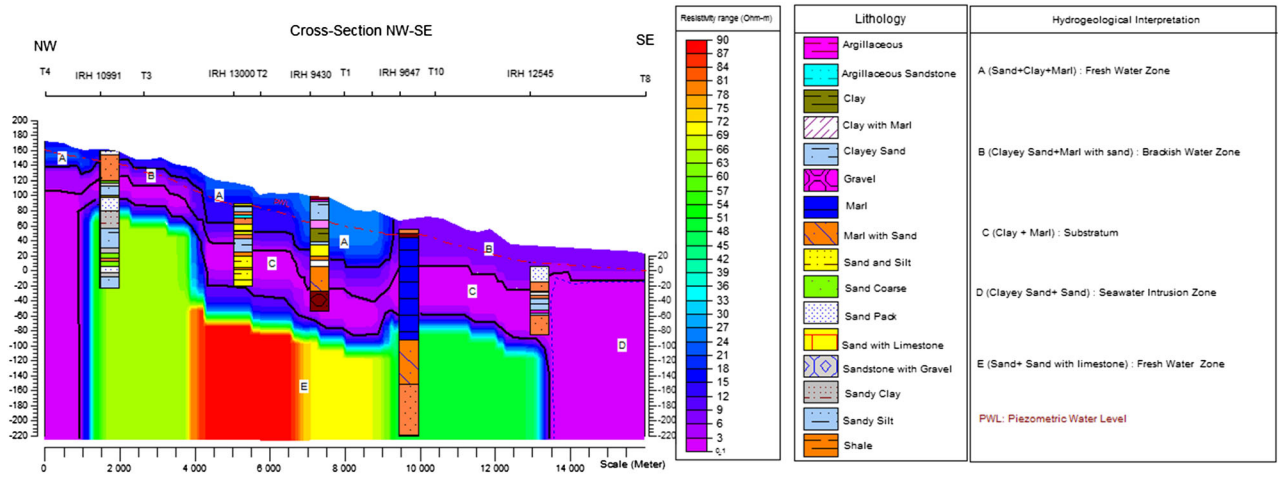

Figure 11. Geoelectrical section (P3)

clay and loam infiltration, fracture filling and washed salts from surface water flooding) (Ernstson and Kirsch, 2006b). Consequently, we assume that in the near surface, the resistivity of freshwater might be affected by the extension of NW–SE fault crossing the Wadi Amroun. Also, it could be due to saturated shale or low-resistivity minerals like gypsum or clay minerals that fill the fault plane running perpendicular to the coast. It should be noted that the Messinian outcropping (Oued El Bir formation) is close to this area (Colleuil, 1976; Fournié, 1978; Bismuth, 1984; Bédir *et al.*, 1996 and Moissette *et al.*, 2010). In addition, this cross fault can be a conduit for seawater (zone D) to move readily towards the water wells.

Apparent iso-resistivity maps

Apparent iso-resistivity maps at different depths. On the basis of the previous TDEM interpretation, six complied maps were constructed at different depths (10, 20, 40, 50, 65 and 100 m) (Figure 12), derived from the Occam smooth-type interpretation of each TDEM sounding. At the depth of 10 m (Figure 12a), relatively high-resistivity materials may represent deposits of sand and gravel with freshwater at some sites. The relatively low-resistivity zones could be attributed to surface clay and silt sediments. At the coastal part, it corresponds to salty water associated with clays and silt close to the coastal area. At the depth of 20 (Figure 12b), there is relatively high-resistivity zone, both at the centre of the valley of Oued El Msan in the east and Oued Lassoued-El Baten in the west. Most probably, these zones represent freshwater coming from Jebel al Rwibia (NE) and Jebel Ech-Chagchag (NW) foothills, respectively, following the drainage pattern of the flood direction, which starts from the northeast and the northwest ends towards the sea (south). The conductive zones at the shallow layers continue and expand with depth. An important conductive zone is close from major faults shown in the geologic map (Figure 1). This low-resistivity expansion reflects the changes associated with fault zone. At a greater depth (40 and 100 m; Figures 12c–12f), there is a very low resistivity at the southwestern part of the study area, in Hammamet South, which starts to show up at 30 m depth. This low resistivity could be attributed to seawater intrusion that might be associated with clays and silt, whereas the high-resistivity values at the northeastern part could be attributed to freshwater zone. However, there is a well-defined boundary between conductive and resistive zones that almost divides the study area into three zones. Both the southern and the northwestern zones have low resistivity, which are attributed to the presence of clays and silt of Plio-Quaternary and Oligo-Eocene deposits, respectively, whereas the northeastern zone has a relatively high resistivity from the conglomerates and the sandstones of Miocene deposits. For all maps, the resistivity values less than 3 Ω·m were attributed to low-permeability materials such as clayey sediments or sediments with a high percentage of clay saturated with salty water. Materials with interpreted resistivity of 5 to 10 Ω·m probably represent sediments with low percentage of clay and with brackish water. Finally, materials with an interpreted resistivity range of 20 to 85 Ω·m probably represent sediments with greater amounts of sand and gravel and freshwater saturated.

Apparent iso-resistivity and iso-depth maps of the salinized zone. The map of iso-resistivity surfaces may estimate the location and the depth of salty water zone. The iso-resistivity map of the salinized zone (Figure 13a) shows two low-resistivity lobes in the southeastern part of the area. The first lobe is just located at El Mammoura zone, measuring a distance at least of 1.5 km. In the north of Nabeul (Dar Chaabene), a second lobe is shown, reaching 5 km far from the coast and indicating the advance of seawater intrusion towards inland. This saltwater encroachment can be probably facilitated by the major surface fault. In addition, between Nabeul and Al Mrazga areas, two great extension lobes are shown, which reach a distance approximately 3 km from the coast. Also, in the touristic zone of the north of Hammamet, the seawater intrusion zone reaches a distance approximately 2 km of the current coast. Throughout the study area, the south of

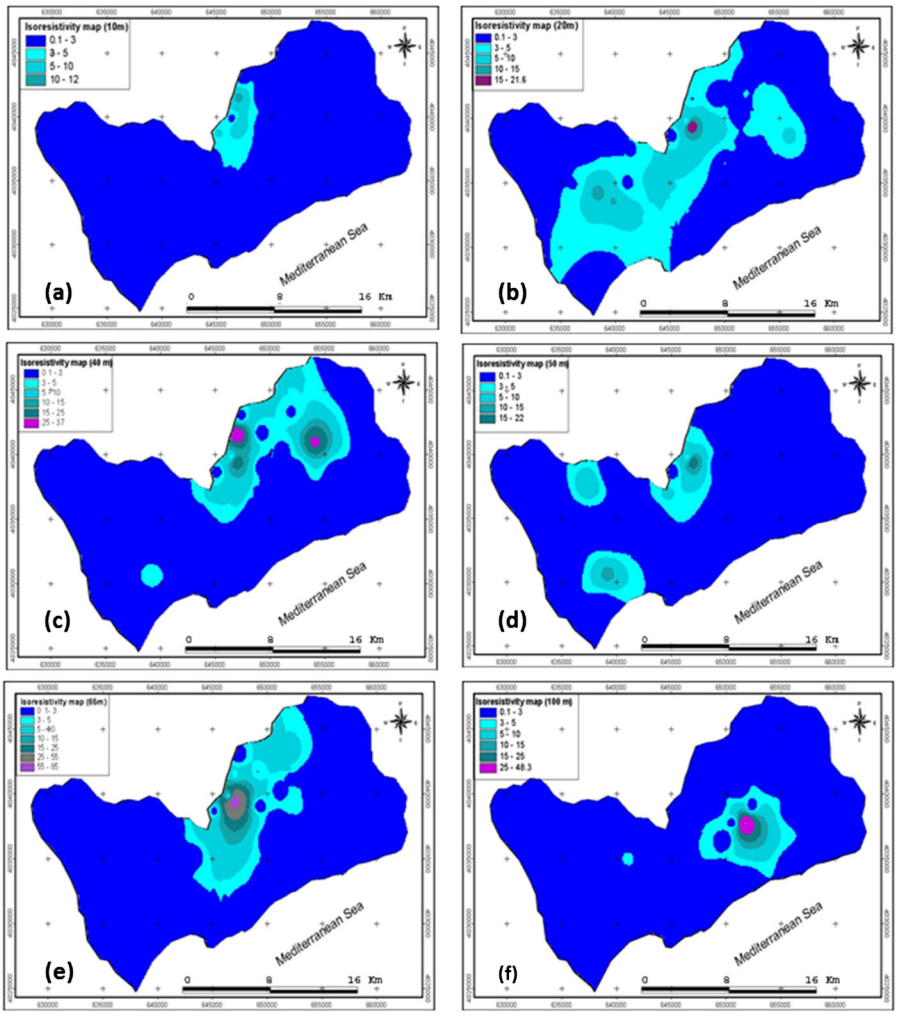

Figure 12. Apparent iso-resistivity maps at (a) 10, (b) 20, (c) 40, (d) 50, (f) 90 and (g) 100 m depth derived from TDEM inversion of smooth models

Hammamet represents the most contaminated zone by seawater intrusion, which can be explained by the upconing of saltwater that may be occurring to excessive withdrawals from local supply wells. Some small zones with relatively high resistivities located along the coast are the consequence of the direct rainwater infiltration through the sandy coastal recent dunes or the Pliocene formation lens (sand and sandstone of Hammamet). In the northwestern part, it shows a great extension of low-resistivity lobe. The groundwater in this zone is saturated with more or less salty to brackish water. This salinization is probably due to the two sources other than seawater intrusion. The first is probably due to the Quaternary (Villafranchian) outcropping rich of clayey sandstone deposits. The second is the effect of the stagnant waters of a hill reservoir (Laziar-Sidi Jedidi) and four hill dams (Guettar, Moussa Chem, Lassoued and Chagcheg) on the groundwater quality.

Thus, the iso-depth map of the salinized zones (Figure 13b) shows that the freshwater–seawater transition zone reaches shallow levels in Nabeul (Dar Chaabene and Sidi El Mehrzi) and Hammamet (the north and south Touristic zone and Bareket Essahel) with 3.5 to 30 m depth. The seawater encroachment occupies a surface relatively limited, but in south Hammamet, the surface occupied by the rise of seawater intrusion is relatively more significant.

Furthermore, the compilation of the spatial distribution of chloride concentration (Figure 14) and the TDEM iso-resistivity map of the salinized zone (Figure 13a) form together a good agreement for the presence of salinized zones in the cited localities of NH area.

On the one hand, far to the coastline (in Bir Bouragba locality), two water samples of shallow wells indicate a chloride content of approximately 78 mg/l and coincide with the TDEM resistivity range between 25 and 40 Ω·m. On the other hand, near the coastline (in the south of Hammamet), TDEM sounding has recorded a very low resistivity of 3.9 Ω·m while the chloride content value is of 2275 mg/l. Also, near the zone of Nabeul–Sidi el Mahrsi, TDEM resistivity is of 5.37 Ω·m, corresponding to high chloride concentrations of approximately 1927.65 mg/l.

Three-dimensional plume

On the basis of the inversion solution of all geoelectromagnetic field data, a 3D model of the spatial distribution of formation resistivities was developed for the area. It is performed using the Environmental Visualisation Software data representation. The program

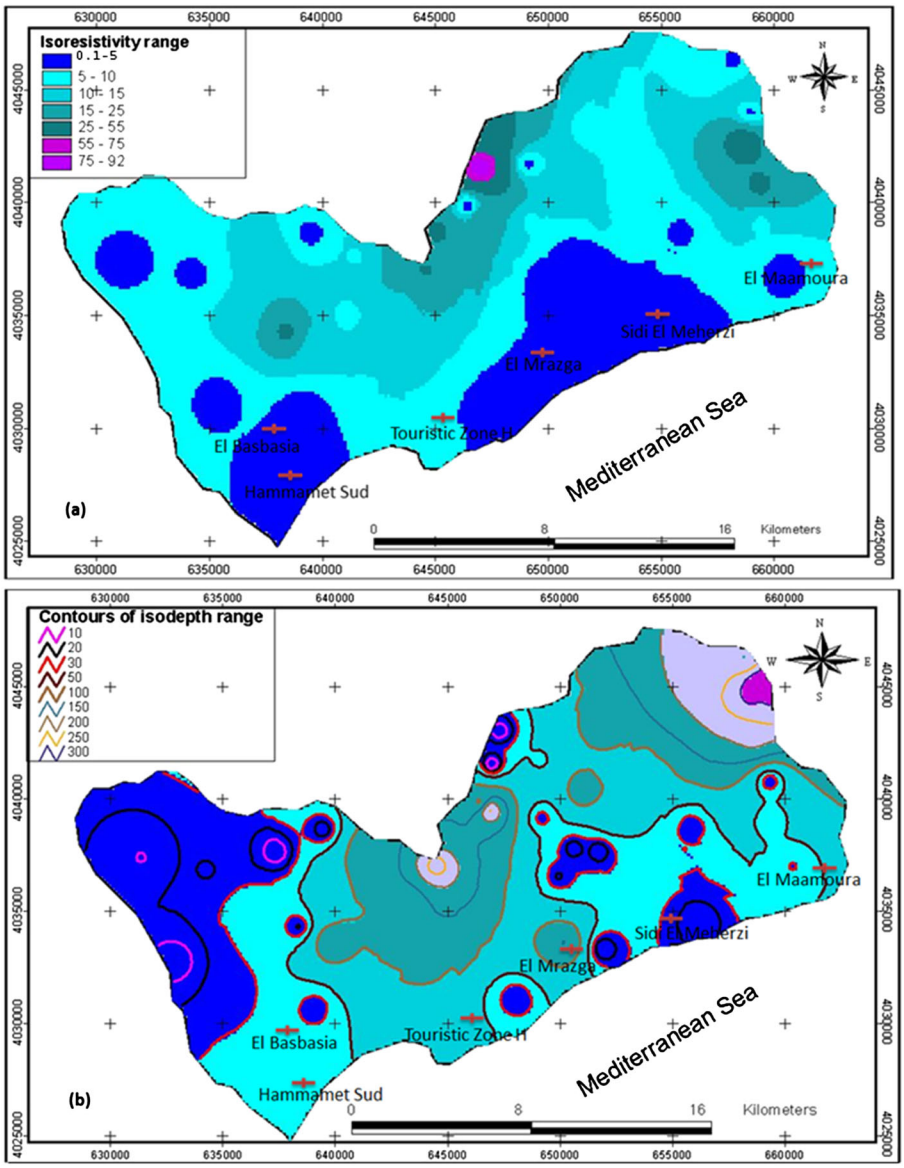

Figure 13. (a) Iso-resistivity map of the salinized zone. (b) Iso-depth map of the salinized zone

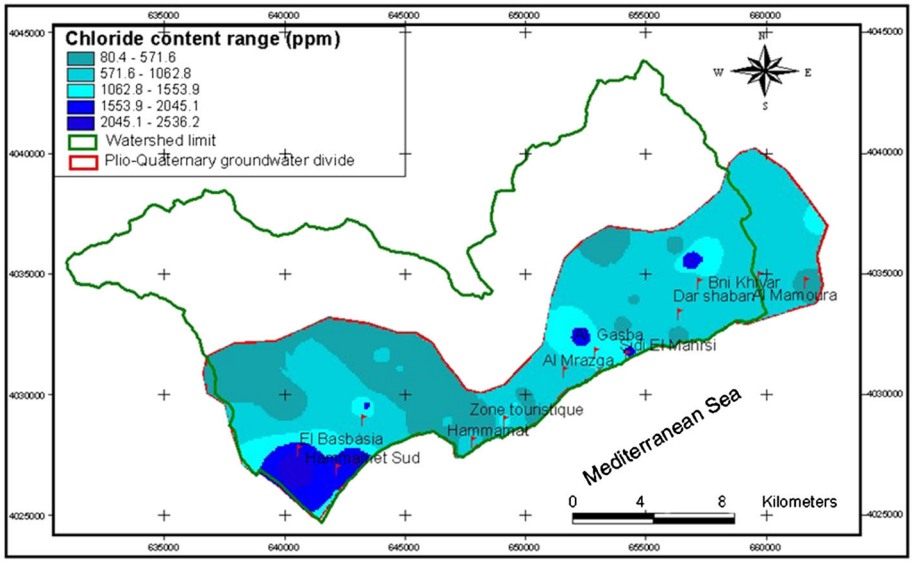

Figure 14. Spatial distribution of chloride concentration evaluated by a hydrogeochemical analysed in the unconfined aquifer of NH

is able to extract data from the entire volume investigated (i.e. resistivities higher, lower than fixed value) and reconstruct the plume or the extension of a layer using 3D interpolation. They revealed a spatial variability of the freshwater–seawater interface with elevation. Figure 15 represents a 3D plume with the formation resistivity between 1 and 5 Ω·m representing a brackish-salty water–saturated zone. However, in the NH coastal plain, closer to Nabeul (Sidi El Mahrzi, El Gasba) and to Hammamet (north and south of touristic zone), a seawater intrusion can be observed. However, towards the inland area, the low-resistivity lobes detected in the western part and to the northward can be attributed to the salty clay nature of the shallow aquifer in these zones.

Furthermore, a small lobe with low resistivity is visualized in the eastern part. It reflects the changes associated with fault zones and probably due to low-resistivity minerals like gypsum or clay minerals that fill the fault plane. The 3D model obtained for the NH basin confirms the previous results deduced from 2D geoelectrical section and iso-resistivity surface maps.

DISCUSSION

The analysis of the previously indicated results reveals different interpretations and assumptions; for example, the coastal geoelectrical section (P2) (Figure 10) shows the distribution of different water types (saline, brackish and fresh). This is consistent with the concept of the classical seawater intrusion phenomenon, described in the coastal zones in which the saltwater wedge is oriented because the coast moves towards the inland with a succession of saline, brackish and freshwater. This conventional configuration of seawater intrusion is not consistently observed in some zones. Different TDEM soundings have shown the presence of saline or brackish water in remote areas of the coast. In the northeastern part, at Dar Chaabene north, the interface of fresh and seawater reached a depth of 22 m in the TDEM sounding (T13), 5 km far from the coast. Towards the south west, precisely at Bareket Essahel, the brackish water reached

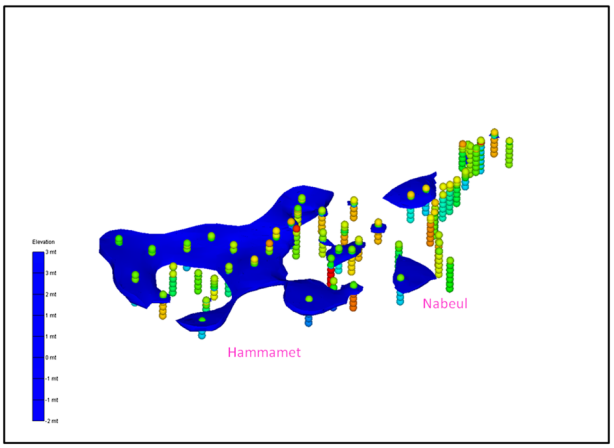

Figure 15. Three-dimensional model of resistivity layer ranging between 1 and 5 Ω·m

23 m in TDEM sounding (T28) and located more than 3.5 km far from the coast.

These TDEM geophysical results are confirmed by the analysis of chloride concentration in the available shallow wells and boreholes in this area (Figure 14). At the north of Nabeul (Dar Chaabene) and Hammamet (Bareket Essahel), the water sample analyses of two shallow wells situated near TDEM sounding locations recorded a chloride concentration of approximately 1690 and 2297 mg/l, respectively.

Near the coastal zone, the absence of salty-brackish water until at least 10.5 m depth is recorded in TDEM sounding (T33) close to the coast, whereas the presence of saline water at 1.5 m depth is recorded in another TDEM sounding (T35). This distribution cannot be explained alone with seawater intrusion concept. The values of chloride concentration in the water samples, of two shallow wells situated at proximity of the previously cited TDEM soundings, reach 110 and 1927 mg/l, respectively.

This study highlights the heterogeneity and complexity of the distribution of freshwater–seawater interface in NH coastal area. The 'sawtooth' distribution of fresh, brackish and salty waters, regardless of the depth of shallow well or borehole, is at odds with the concept of seawater intrusion. However, in the classic model of seawater wedges, several geological sources can affect coastal groundwater quality (Custodio, 1997; Barlow, 2003). These sources include the following: (i) the migration of subsurface saline water through faults, fractures or permeable geologic units where driven by gravity or fluid pressure; (ii) the entrapped fossil seawater in the unflushed parts of an aquifer, in which such water was either trapped in sedimentary formations when they were deposited (connate water) or flowed into the formations during periods of relatively high sea levels when seawater flooded low-lying coastal areas; and (iii) the dissolution of evaporitic deposits such as halite (rock salt), anhydrite and gypsum (Barlow, 2003).

Moreover, the interpretation of TDEM geoelectrical sections and iso-resistivity maps allows us to confirm the presence of major normal fault-directed NW–SE crossing the eastern part of the study area (Ben Salem, 1992) and to identify new faults overlain by Plio-Quaternary deposits. This major fault was created during a tectonic activity from the Pliocene to the present and was interpreted as being responsible for a considerable displacement of a major part of quaternary deposits (Castany, 1948; Chihi, 1995; Ben Salem, 1992). However, the geoelectrical section P3 (Figure 11) shows that in both zones of Dar Chaabene north and El Maamoura, low-resistivity anomalies have been visualized and aligned along the southern extension of the cited major fault located near the coast. The TDEM sounding (T13) carried out in the north of Dar Chaabene presents a resistivity of 12.43 Ω·m at 12.25 m depth. The TDEM sounding (T16) localized in the El Maamoura zone reveals a resistivity of 11 Ω·m at 11.5 m depth. On the other side, the TDEM sounding (T14) located in the

northern part of this fault shows that the ground is saturated with freshwater up to at least 64 m and with a resistivity of 46.53 Ω·m. In addition, the presence of brackish water in this area is confirmed by the high value of chloride concentration, where the values of 2297 and 878 mg/l are recorded in the two shallow wells of Dar Chaabene north and El Maamoura, respectively. Two hypotheses can be conducted on the origin of these low-resistivity and brackish waters detected in this eastern part of study area. First, the low-resistivity is due to open water-filled fissures; the resistivity within a fault or fracture zone is in general lower than the resistivity of the hard rock. Clay and silt infiltration through the fault plane and fractures leads to low resistivities but on the other hand strongly reduces hydraulic conductivities (Ernstson and Kirsch, 2006b). Consequently, the origin of salty-brackish water of Dar Chaabene north is the marine Messinian deposits (upper Miocene) of Oued el Bir formation trapped in the open fissures of this major fault. These deposits consist of sands, sandstones, clays and gypsum (Moissette *et al*., 2010). The seawater invasion interests permeable rocks for fractures. Hence, the second hypothesis is that the cited major fault seems to make the rock very permeable perpendicular to the coastline and to provide a conduit for seawater to move readily towards the wells. In the western part, two TDEM soundings (T29 and T30) are localized at 6 and 9 km, respectively, far from the coast and on Villafranchian Quaternary deposits. These TDEM soundings show the resistivity of approximately 9.78 and 7.39 Ω·m at depths lower than 21.5 and 116.5 m, respectively. The water samples of two shallow water wells situated at close of these TDEM soundings show values of chloride concentrations at 113.6 and 195.25 mg/l, respectively. This leads to the assumption that the recorded low resistivity is probably due to another source than seawater intrusion. It is probably attributive of the lithological nature of clayey sandstone shallow aquifer in this area.

CONCLUSION

The stratigraphic section of the coastal plain of NH region consists of a complex blend of several lithologies, which are heterogeneous aquifers of sand and limestone containing highly variable amounts of both dispersed and interbeded clays and/or separated by sandy clay confining beds. Hence, the freshwater zone containing a high percentage of clays has lower apparent resistivity than clean sand or limestone aquifer. Both clay and saline pore fluids can suppress the bulk resistivity of aquifer, and the unknotting of the two signals is one of the more challenging aspects of interpreting data from a TDEM sounding. This problem is best resolved in this study by the correlation of TDEM resistivity logs with borehole logging data, which are also calibrated with the chloride content results of water samples from neighbouring boreholes and shallow wells. Also, 2D geoelectrical sections, both iso-resistivity and iso-depth maps of salinized zone, 3D plume and distribution of chloride concentration map were established. All results were compiled, interpreted with a thorough understanding of the local and regional geological settings and provided additional information on the regional hydro-lithostratigraphic data of the Plio-Quaternary aquifer of NH, especially on the distribution of freshwater–seawater transition zone. Therefore, the salinized zones are detected closer to the Nabeul region (Sidi Moussa, Sidi El Mahrsi, Al Gasba and Mrazgua) and the Hammamet region (Touristic zone of Hammamet north, Baraket Essahel and Hammamet Sud).

The vertical transition from fresh to salty conditions may not be abrupt but can occur over a fairly broad depth range of several metres to tens of metres. The TDEM resistivity values within a transition zone may range from ~1 to 5 Ω·m, depending on the chloride concentration, the clay content, the porosity and the presence of other dissolved solids.

In this study, different hypotheses were proposed to explain the relationship between the litho-structural context and the water salinization of NH aquifer. The seawater intrusion is directly dependent on the geometry, geology and hydrodynamic characteristics of the NH aquifer, as reflected by its heterogeneous nature. Furthermore, this study points out the juxtaposition of deep saline intrusions, demonstrating that the concept of a homogeneous wedge-shaped body parallel to the seashore can no longer be used to describe the NH aquifer. Indeed, TDEM profiling provided additional information on the relation between tectonic events and saline water intrusion. Saltwater seems to follow preferential intrusion directions corresponding to fault rather than the classic model of a salt wedge. These results suggest the hypothesis that the seawater intrusion relates to the tectonic configuration of the aquifer. The presence of a seawater front located far from the coast, as indicated by TDEM soundings, could be explained by the geological history of the NH area. Finally, seawater intrusion and saltwater transport phenomena typically produce electrical conductivity contrasts in the subsurface. Results of this study reveal that TDEM method is powerful tool to map these contrasts, to detect freshwater–seawater transition zone and to monitor hydrogeology conditions in the complex and heterogeneous geological setting of coastal groundwater environments.

ACKNOWLEDGEMENTS

This work was conducted as part of cooperative research studies between the Faculty of Engineering of Cagliari in Italy and the National Institute of Agronomy (INAT) in framework of Interlink project of Italian Ministry of Research, coordinated by Prof. Gaetano Ranieri. Special thanks are due to the local groundwater management authority (CRDA Nabeul) for providing hydrogeological data. We are grateful to the Geophysics laboratory at the Faculty of Engineering at University of Cagliari who

provided significant logistic and financial support. Sincere thanks are also due to the anonymous reviewers for their helpful comments and suggestions, which improved the quality of this manuscript.

REFERENCES

Barlow PM. 2003. Ground Water in Freshwater-Saltwater Environments of the Atlantic Coast. U.S. Geological Survey, Reston, Virginia. *Circular* **1262**: 121.

Bédir M, Tlig S, Bobier C, Aissaoui N. 1996. Sequence stratigraphy, basin dynamics and petroleum geology of the Miocene from Eastern Tunisia. *Am Assoc Petrol Geol Bull* **80**(1): 63–81.

Ben Ayed N. 1986. *Evolution tectonique de l'avant pays de la chaîne alpine de Tunisie du début du Mésozoïque à l'Actuel*, Thèse Sciences, Université Paris Sud: Orsay, France; pp 327.

Ben Salem H, Colleuil B. 1991. Carte géologique de la Tunisie à l'échelle 1/ 50.000, Feuille de Nabeul n° 30.

Ben Salem H. 1992. Contribution à la connaissance de la géologie du Cap Bon: Stratigraphie, Tectonique et Sédimentologie. Thèse 3ème cycle Faculté des Sciences de Tunis, Université de Tunis II: pp 144.

Bismuth H. 1984. Les unités lithostratigraphiques du Miocène en Tunisie orientale. Société des Sciences de la Terre de Tunisie, Tunis, p. 3.

Blondel T. 1991. *Les séries à tendance régressive marine du Miocène inférieur à moyen en Tunisie centrale*, Thèse ès-Sciences Gèologiques: Université de Genève; pp 487.

Buckley DK, Hinsby K, Manzano M. 2001. Application of geophysical borehole logging techniques to examine coastal aquifer. Palaeohydrogeology. In *Palaeowaters in coastal Europe. Evolution of groundwater since the late Pleistocene*, Vol. **189**, Edmunds WM, Milne CJ (eds). Geological Society: London, Special Publication; 251–270.

Burollet PF. 1956. Contribution à l'étude stratigraphique de la Tunisie centrale. *Annales Mines et Géologie Tunis* **18**: 195–203.

Castany G. 1948. Les fossés d'effondrement de Tunisie. *Ann. Min. Geol. Tunis*, p 3.

Chakroun A, Zaghbib-Turki D, Moigne AM, De Lumley H. 2005. Découverte d'une faune de mammifère du Pléisticène supérieur dans la grotte d'El Geffel (Cap-Bon, Tunisie). *CR Palevol* **4**: 317–325.

Chihi L. 1995. Les fossés néogènes à quaternaire de la Tunisie et de la mer pélagienne: une étude structurale et une signification dans le cadre géodynamique de la Méditerranée centrale. Thèse de Doctorat ès Sciences Géologiques. Univ de Tunis II. Fac Sc Tunis, pp 324.

Choudhury K, Saha DK. 2004. Integrated geophysical and chemical study of saline water intrusion. *Ground Water* **42**(5): 671–677.

Christensen NB. 1995. 1D imaging of central loop transient electromagnetic soundings. *J Environ Eng Geophys* 53–66.

Christensen NB, Sørensen KI. 1998. Surface and borehole electric and electromagnetic methods for hydrogeophysical investigations. *European Journal of Environmental and Engineering Geophysics* **3**(1): 75–90.

Colleuil B. 1976. Etude stratigraphique et néotectonique des formations néogènes et quaternaires de la région Nabeul–Hammamet (Cap Bon, Tunisie). Mémoire de D.E.S, pp 94.

Constable S, Parker R, Constable C. 1987. Occam's inversion. A practical algorithm for generating smooth models from electromagnetic sounding data. *Geophysics* **52**(3): 289–300.

Custodio E. 1997. Detection, chap. 2 in Seawater intrusion in coastal aquifers—Guidelines for study, monitoring and control: Rome, Italy, Food and Agriculture Organization of the United Nations. *Water Reports* **11**: 6–22.

Danielsen JE, Auken E, Jorgensen F, Søndergaard VH, Sørensen KI. 2003. The application of the transient electromagnetic method in hydrogeophysical surveys. *Journal of Applied Geophysics* **53**: 181–198.

De Breuk W, De Moor G. 1969. The water table aquifer in the eastern coastal area of Belgium. *Bull. Assoc. Sci. Hydro* **14**: 137–155.

Duque C, Calvache M, Pedrera A, Martı´n-Rosales W, Lo´pez-Chicano M. 2008. Combined time domain electromagnetic soundings and gravimetry to determine marine intrusion in a detrital coastal aquifer (Southern Spain). *Journal of Hydrology* **349**: 536–547.

DWR, District of the Water Resources of Nabeul. 2005. Annuaire d'exploitation des nappes phréatiques.

Ebraheem AAM, Senosy MM, Dahab KA. 1997. Geoelectrical and hydrogeochemical studies for delineating ground-water contamination due to salt-water intrusion in the northern part of the Nile Delta, Egypt. *Ground Water* **35**(2): 216–222.

Elmejdoub N, Jedoui Y. 2009. Pleistocene raised marine deposits of the Cap Bon peninsula (N-E Tunisia): records of sea-level highstands, climatic changes and coastal uplift. *Geomorphology* **112**:179–189.

Ernstson K, Kirsch R. 2006a. The transient electromagnetic methods. In *Groundwater geophysics: a tool for hydrogeology*, Krisch R (ed). Springer: Berlin; 179–226.

Ernstson K, Kirsch R. 2006b. Aquifer structures: fracture zones and caves. In *Groundwater geophysics: a tool for hydrogeology*, Krisch R (ed). Springer: Berlin; 447–474.

Everett M, Meju M. 2005. Near surface controlled-source electromagnetic induction: background and recent advances. In *Hydrogeophysics*, Rubin Y, Hubbard S (eds). Springer: The Netherlands.

Fainberg E. 1999. *TEM FAST 48 manual*. Applied Electromagnetic Research (AEMR): the Netherlands.

Fitterman DV, Stewart MT. 1986. Transient electromagnetic soundings for groundwater. *Geophysics* **51**: 995–1006.

Fournié D. 1978. Nomenclature lithostratigraphique des séries du Crétacé supérieur au Tertiaire de Tunisie. *Bull. Centr. Rech. Explor. Prod. Elf-Aquitaine* **2**: 97–114.

Frohlich RK, Urish DW, Fuller J, Reilly MO. 1994. Use of geoelectrical method in groundwater pollution surveys in a coastal environment. *Journal of Applied Geophysics* **32**: 139–154.

Ginsberg A, Levanton A. 1976. Determination of saltwater interface by electrical resistivity sounding. *Hydrological Science Bulletin* **21**: 561–568.

Goldman M. 1988. Transient electromagnetic inversion based on an approximate solution to the forward problem. *Geophysics* **53**: 118–128.

Goldman M, Gilad D, Ronen A, Melloul A. 1991. Mapping of seawater intrusion into the coastal aquifer of Israel by the time domain electromagnetic method. *Geoexploration* **28**: 153–174.

Goldman M, Neubauer F. 1994. Groundwater exploration using integrated geophysical techniques. *Surveys in Geophysics* **15**: 331–361.

Gottwein PB, Gondwe BN, Christiansen L, Herckenrath D, Kgotlhang L, Zimmermann S. 2010. Hydrogeophysical exploration of three-dimensional salinity anomalies with the time-domain electromagnetic method (TDEM). *Journal of Hydrology* **380**: 318–329.

Hodlur GK, Dhakate R, Sirisha T, Panaskar DB. 2010. Resolution of freshwater and saline water aquifers by composite geophysical data analysis methods. *Hydrological Sciences Journal* **55**(3): 414–434.

Hoekstra P, Bloom M. 1986. Case histories of time domain electromagnetic soundings in environmental geophysics. In *Geotechnical and Environmental Geophysics*, vol. **2**, Ward S (ed). SEG: Tulsa, OK; 1–15.

Hwang S, Shin J, Park I, Lee S. 2004. Assessment of seawater intrusion using geophysical well logging and electrical soundings in a coastal aquifer. Youngkwang-gun, Korea. *Exploration Geophysics* **35**: 99–104.

Jorgensen DG, Petricola M. 1995. Research borehole geophysical logging in determining geohydrologic properties. *Ground Water* **33**(4): 589–596.

Kafri U, Goldman M, Lang B. 1997. Detection of subsurface brines, freshwater bodies and the interface configuration in between by the Time Domain Electromagnetic (TDEM) method in the Dead Sea rift, Israel. *J. Env. Geol* **31**: 42–49.

Kafri U, Goldman M. 2005. The use of time domain electromagnetic method to delineate saline groundwater in granular and carbonate aquifers and to evaluate their porosity. *Journal of Applied Geophysics* **57**: 167–178.

Kaufman AA, Keller GV. 1983. *Frequency and Transient Soundings*. Elsevier: Amsterdam.

Keating PB, Crossley DJ. 1990. The inversion of time-domain electromagnetic data using the finite plate model. *Geophysics* **55**: 705–711.

Keller GV, Frischknecht FC. 1966. *Electrical Methods in Geophysical Prospecting*. Pergamon: NY.

Kerrou J, Renard P, Tarhouni J. 2010. Status of the Korba groundwater resources (Tunisia): observations and three-dimensional modelling of seawater intrusion *Hydrogeology Journal* **18**: 1173–1190.

Keys WS. 1997. *A practical guide to borehole geophysics in environmental investigations*. Lewis Publishers: Boca Raton, Florida.

Kobr M, Mares S, Paillet F. 2005. Geophysical well logging—Borehole geophysics for hydrogeological studies: Principles and applications. In *Hydrogeophysics*, Rubin Y, Hubbard SS (eds). Springer: Amsterdam; 291–331.

Kouzana L, Ben Mammou A, Sfar Felfoul M. 2009. Seawater intrusion and associated processes: case of the Korba aquifer (Cap-Bon, Tunisia). *CR Geosci* **341**: 21–35.

Macnae JC, Lamontagne Y, West GF. 1984. Noise processing techniques for time domain EM systems. *Geophysics* **49**: 934– 948.

Mares S, Zboril A, Kelly WE. 1994. Logging for the determination of aquifer hydraulic properties. *The Log Analyst* **35**(6): 28–36.

Maute RE. 1992. Electrical logging: State-of-theart. *The Log Analyst* **33**(3): 206–227.

McCracken KG, Oristaglio ML, Hohmann GW. 1986. The minimization of noise in electromagnetic exploration systems. *Geophysics* **51**: 819–832.

Meyers GD. 1992. A Review of Nuclear Logging. *The Log Analyst* **33**(3): 228–238.

Moissette P, Cornée JJ, Mannaï-Tayech B, Rabhi M, André JP, Koskeridou E, Méon H. 2010. The western edge of the Mediterranean Pelagian Platform: A Messinian mixed siliciclastic–carbonate ramp in northern Tunisia. *Palaeogeography Palaeoclimatology Palaeoecology* **285**: 85–103.

Nabighian MN. 1979. Quasistatic transcient response of a conducting halfspace. An approximate representation. *Geophysics* **44**: 1700–1705.

Nassir ASS, Loke MH, Lee CY, Nawawi MNM. 2000. Salt–water intrusion mapping by geoelectrical imaging surveys. *Geophysical Prospecting* **48**: 647–661.

Nowroozi AA, Horrocks SB, Henderson P. 1999. Saltwater intrusion into freshwater aquifer in the eastern shore of Virginia: A reconnaissance electrical resistivity survey. *Journal of Applied Geophysics* **42**: 1–22.

Ozer A, Pskoff R, Sanlaville P, Ulzega A. 1980. Essai de corrélation du Pléistocène supérieur de la Sardaigne et de la Tunisie. *CR Acad. Sci. Paris, Ser D* **291**: 801–804.

Paine JG. 2003. Determining salinization extent, identifying salinity sources, and estimating chloride mass using surface, borehole, and airborne electromagnetic induction methods. *Water Resources Research* **39**(3): 1–10.

Palacky GI. 1987. Resistivity characteristics of geological targets. In *Electromagnetic Methods in Applied Geophysics-Theory*, Nabighian, M (ed). Society of Exploration Geophysicists: Tulsa, OK; 53–129.

Paniconi C, Khlaifi I, Lecca G, Giacomelli A, Tarhouni J. 2001. Modeling and analysis of seawater intrusion in the coastal aquifer of eastern Cap-Bon, Tunisia. *Transport Porous Med* **43**: 3–28.

Raiche AP. 1984. The effect of ramp function turn-off on the TEM response of a layered ground. *Exploration Geophysics* **15**: 37–41.

Ranieri G. 2000. Tem Fast: a useful tool for hydrogeologists and environmental engineers. *Annali di Geofisica* **43**(6): 1147–1158.

Repsold H. 1989. *Well Logging in Groundwater Development*. International Contributions to Hydrogeology, vol. **9**. International Association of Hydrogeologists, Verlag Heinz Heise: Hannover; 136 p.

Sabet MA. 1975. Vertical electrical resistivity sounding locate groundwater resources: a feasibility study. Virginia Polytechnical Institute. *Water Resources Bulletin* **73**: 63.

Sherif M, El Mahmoudi A, Garamoon H, Kacimov A, Akram S, Ebraheem A, Shetty A. 2006. Geoelectrical and hydrogeochemical studies for delineating seawater intrusion in the outlet of Wadi Ham, UAE. *Environmental Geology* **49**: 536–551.

Spies BR. 1996. Electrical and electromagnetic borehole measurements. *Surveys in Geophysics* **17**: 517 –556.

Trabelsi F, Tarhouni J, Ben Mammou A, Ranieri G. 2011. GIS-based subsurface databases and 3-D geological modelling as a tool for the set-up of hydrogeological framework: Nabeul–Hammamet coastal aquifer case study (Northeast Tunisia). *Environ Earth Sci* DOI: 10.1007/s12665-011-1416-y.

Turki MM. 1985. Poly cinématique et contrôle sédimentaire associé sur la cicatrice de Zahouan-Nebhana. Thèse d'Etat, Faculté des sciences de Tunis.

Urish DW, Frohlich RK. 1990. Surface electrical resistivity in coastal groundwater exploration. *Geoexploration* **26**: 267–289.

Van Dam JC, Meulenkamp, JJ. 1967. Some results of the geo-electrical resistivity method in groundwater investigations in The Netherlands. *Geogphysical Prospecting* **15**(1): 92–115.

Wilson SR, Ingham M, McConchie JA. 2005. The applicability of the earth resistivity methods for saline interface definition. *Journal of Hydrology* **316**: 301–312.

Xue Y, Wu J, Lui P, Wang J, Jiang Q, Shi H. 1993. Sea-water intrusion in the coastal area of the Laizhou Bay, China: 1. Distribution of seawater intrusion and its hydrochemical characteristics. *Ground Water* **31**(4): 532–537.

Yechieli Y, Kafri U, Goldman M, Voss CI. 2001. Factors controlling the configuration of the fresh–saline water interface in the Dead Sea coastal aquifers. *Hydrogeology Journal* **9**:367–377.

Zohdy AAR. 1969. The use of Schlumberger and equatorial soundings on ground water investigations near El Paso, TX. *Geophysics* **34**: 713–728.

